Hindawi Publishing Corporation
EURASIP Journal on Wireless Communications and Networking
Volume 2009, Article ID 568570, 11 pages
doi:10.1155/2009/568570

Research Article

Feedforward Data-Aided Phase Noise Estimation from a DCT Basis Expansion

Jabran Bhatti and Marc Moeneclaey

Department of Telecommunications and Information Processing, Ghent University, 9000 Ghent, Belgium

Correspondence should be addressed to Marc Moeneclaey, marc.moeneclaey@telin.ugent.be

Received 1 July 2008; Revised 5 November 2008; Accepted 25 December 2008

Recommended by Erchin Serpedin

This contribution deals with phase noise estimation from pilot symbols. The phase noise process is approximated by an expansion of discrete cosine transform (DCT) basis functions containing only a few terms.We propose a feedforward algorithm that estimates the DCT coefficients without requiring detailed knowledge about the phase noise statistics. We demonstrate that the resulting (linearized) mean-square phase estimation error consists of two contributions: a contribution from the additive noise, that equals the Cramer-Rao lower bound, and a noise independent contribution, that results from the phase noise modeling error. We investigate the effect of the symbol sequence length, the pilot symbol positions, the number of pilot symbols, and the number of estimated DCT coefficients on the estimation accuracy and on the corresponding bit error rate (BER). We propose a pilot symbol configuration allowing to estimate any number of DCT coefficients not exceeding the number of pilot symbols, providing a considerable performance improvement as compared to other pilot symbol configurations. For large block sizes, the DCT-based estimation algorithm substantially outperforms algorithms that estimate only the time-average or the linear trend of the carrier phase.

1. Introduction

Phase noise refers to random perturbations in the carrier phase, caused by imperfections in both transmitter and receiver oscillators. Compensation of this phase noise is critical since these disturbances can considerably degrade the system performance. The phase noise process typically has a low-pass spectrum [1]. A description of the characteristics of oscillator phase noise is given in [2]. Discrete-time processes that have a bandwidth which is considerably less than the sampling frequency can often be modeled as an expansion of suitable basis functions, that contains only a few terms. Such a basis expansion has been successfully applied in the context of channel estimation and equalization in wireless communications, where the coefficients of the channel impulse response are low-pass processes with a bandwidth that is limited by the Doppler frequency [3–5]. Several methods trying to tackle the phase noise problem exist.

(i) Designing oscillators operating at low-phase noise reduces the need of accurate phase noise compensation algorithms. This, however, leads to expensive oscillators which are difficult to integrate on chip [6–8].

(ii) Phase noise can be tracked by means of a feedback algorithm that operates according to the principle of the phase-locked loop (PLL). As feedback algorithms give rise to rather long acquisition transients, they are not well suited to burst transmission systems [9, 10].

(iii) The observation interval is divided into subintervals and a feedforward algorithm is used to estimate within each subinterval the local time-average (or the linear trend) of the phase [9–11]. This corresponds to approximating the phase noise by a function that is constant (or linear) within each subinterval. Such algorithms avoid the long acquisition transients encountered with feedback algorithms. However, in order that the piecewise constant (or linear) approximation of the phase noise be accurate, the subintervals should be short, in which case a high sensitivity to additive noise occurs.

(iv) Recently, iterative joint estimation and decoding/detection algorithms have been proposed that make use of the a priori statistics of the phase noise process. A factor graph approach for the estimation of the Markov-type phase noise has been presented in [12, 13], while in [14, 15] sequential Monte Carlo methods combined with Kalman filtering are used to perform detection in the presence of phase noise. These algorithms are computationally rather complex, prevent the use of off-the-shelf decoders, and assume detailed knowledge about the phase noise statistics at the receiver. Less complex iterative phase noise estimation algorithms based on Wiener filtering have been presented in [16], but still require knowledge about the phase noise autocorrelation function at the receiver.

In this contribution, we apply the basis expansion model to the problem of phase noise estimation from pilot symbols only, using the orthogonal basis functions from the discrete cosine transform (DCT). In contrast to the case of channel estimation, the phase noise does not enter the observation model in a linear way. Section 2 presents the system description which includes the observation model and a general phase noise model. Also, the phase noise estimation algorithm, based on the estimation of only a few DCT coefficients, is derived. Section 3 contains the performance analysis of the proposed algorithm in terms of the mean-square error (MSE) of the phase estimate. The behavior of the linearized model in the frequency domain is examined in Section 4. Analysis results are confirmed by computer simulations in Section 5, which consider both the mean-square phase estimation error and the associated bit error rate (BER) degradation. Section 6 gives a complexity analysis of our algorithm. Conclusions are drawn in Section 7.

2. System Description

We consider the transmission of a block of K data symbols over an AWGN channel that is affected by phase noise. The resulting received signal is represented as

$$r(k) = a(k)e^{j\theta(k)} + w(k) \quad \text{for } k = 0,\ldots,K-1, \tag{1}$$

where the index k refers to the kth symbol interval of length T, $\{a(k)\}$ is a sequence of data symbols with symbol energy $E[|a(k)|^2] = E_s$, the additive noise $\{w(k)\}$ is a sequence of i.i.d. zero-mean circularly symmetric complex-valued Gaussian random variables with $E[|w(k)|^2] = N_0$, and $\theta(k)$ is a time-varying phase noise process with $K\times K$ correlation matrix $\mathbf{R}_\theta$. The symbol sequence $\{a(k)\}$ contains K_P known pilot symbols at positions $k_i, i = 0,\ldots,K_P-1$, with constant magnitude $|a(k_i)|^2 = E_s$. From the observation of the received signal at the pilot symbol positions k_i, an estimate $\hat{\theta}(k)$ of the time-varying phase $\theta(k)$ is to be produced. This phase estimate will be used to rotate the received signal before data detection, that is, the detection of the data symbols is based on $\{z(k)\} = \{r(k)\exp(-j\hat{\theta}(k))\}$. The detector is designed under the assumption of perfect carrier synchronization, that is, $\hat{\theta}(k) = \theta(k)$. For uncoded transmission, the detection algorithm reduces to symbol-by-symbol detection:

$$\hat{a}(k) = \arg\min_{a\in A}\left|z(k) - a\right|^2, \quad k \notin \{k_i, i = 0,\ldots,K_P-1\} \tag{2}$$

with A denoting the symbol constellation. The phase $\theta(k)$ can be represented as a weighed sum of K basis functions over the interval $[0, K-1]$:

$$\theta(k) = \sum_{n=0}^{K-1} x_n\psi_n(k), \quad k = 0,\ldots,K-1. \tag{3}$$

As $\theta(k)$ is essentially a low-pass process, it can be well approximated by the weighed sum of a *limited number* $N(\ll K)$ of suitable basis functions:

$$\theta(k) \approx \sum_{n=0}^{N-1} x_n\psi_n(k), \quad k = 0,\ldots,K-1. \tag{4}$$

In this contribution, we make use of the orthonormal discrete cosine transform (DCT) basis functions, that are defined as

$$\psi_n(k) = \begin{cases} \sqrt{\dfrac{1}{K}}, & n = 0, \\ \sqrt{\dfrac{2}{K}}\cos\left(\dfrac{\pi n}{K}\left(k+\dfrac{1}{2}\right)\right), & n > 0. \end{cases} \tag{5}$$

Hence, from (3), x_n is the nth DCT coefficient of $\theta(k)$. As $\psi_n(k)$ has its energy concentrated near the frequencies $n/2KT$ and $-n/2KT$, the DCT basis functions are well suited to represent a low-pass process by means of a small number of basis functions.

In the following, we produce from the observation $\{r(k_i)\}$ at the pilot symbol positions k_i, with $i = 0,\ldots,K_P-1$, an estimate $\hat{x}_n$ of the coefficients x_n, with $n = 0,\ldots,N-1$, using the phase model (4) with equality. The final estimate $\hat{\theta}(k)$ is obtained by computing the inverse DCT of $\{\hat{x}_n\}$:

$$\hat{\theta}(k) = \sum_{n=0}^{N-1} \hat{x}_n\psi_n(k) \quad \text{for } k = 0,\ldots,K-1. \tag{6}$$

However, as (4) is not an exact model of the true phase $\theta(k)$, the phase estimate is affected not only by the additive noise contained in the observation, but also by a phase noise modeling error. Considering the observations (1) at instants k_i, and assuming that (4) holds with equality, we obtain

$$\mathbf{r}_P = \mathbf{D}(\mathbf{x})\mathbf{a}_P + \mathbf{w}_P, \tag{7}$$

where for $i = 0,\ldots,K_P-1$; $(\mathbf{r}_P)_i = r(k_i)$, $(\mathbf{w}_P)_i = w(k_i)$, $(\mathbf{a}_P)_i = a(k_i)$, and $\mathbf{D}(\mathbf{x})$ is a $K_P \times K_P$ diagonal matrix with

$$\left(\mathbf{D}(\mathbf{x})\right)_i = e^{j(\mathbf{\Psi_P x})_i} \tag{8}$$

and $(\mathbf{\Psi_P})_{i,n} = \psi_n(k_i)$, $(\mathbf{x})_n = x_n$, $n = 0,\ldots,N-1$ with $N \le K_P$. The $K_P \times 1$ vectors $\mathbf{r_P}$, $\mathbf{a_P}$, and $\mathbf{w_P}$ can be viewed as resulting from subsampling $\{r(k)\}$, $\{a(k)\}$, and $\{w(k)\}$ at the instants k_i that correspond to the pilot symbol positions. Similarly, the nth column of the $K_P \times N$ matrix $\mathbf{\Psi_P}$ is obtained by subsampling the n th DCT basis function $\psi_n(k)$. Maximum likelihood estimation of $\mathbf{x}$ from $\mathbf{r}_P$ results in

$$\widehat{x}_{ML} = \arg\min_{\mathbf{x}} \left| \mathbf{r}_P - \mathbf{D}(\mathbf{x})\mathbf{a_P} \right|^2. \tag{9}$$

As $\mathbf{x}$ enters the observation $\mathbf{r}_P$ in a nonlinear way, the ML estimate is not easily obtained. Therefore, we resort to a suboptimum ad hoc estimation of $\mathbf{x}$, which is based on the argument (angle) of the complex-valued observations. However, as the function $\arg(z)$ reduces the argument of z to an interval $[-\pi, \pi]$, taking $\arg(r(k_i))$ might give rise to phase wrapping, especially when the time-average of $\theta(k)$ is close to $-\pi$ or π. In order to reduce the probability of phase wrapping, we first rotate the observation $\mathbf{r}$ over an angle θ_{avg} that is close to the time-average of $\theta(k)$, then we estimate the DCT coefficients of the fluctuation $\theta(k) - \theta_{\text{avg}}$ and finally we compute the phase estimate $\widehat{\theta}(k)$. We select

$$\theta_{\text{avg}} = \arg\left(\sum_{i=0}^{K_P-1} r(k_i)\right) \tag{10}$$

and construct $\mathbf{r}'$ with

$$\begin{aligned}(\mathbf{r}')_i &= r'(k_i) \\ &= \arg\left(r(k_i)a^*(k_i)\exp(-j\theta_{\text{avg}})\right) \\ &\qquad \text{for } i = 0,\ldots,K_P-1.\end{aligned} \tag{11}$$

We obtain an estimate $\widehat{\mathbf{x}}'$ of the DCT coefficients of the fluctuation $\theta(k) - \theta_{\text{avg}}$ through a least-squares fit $\widehat{\mathbf{x}}' = \arg\min_{\mathbf{x}} |\mathbf{r}' - \mathbf{\Psi_P}\mathbf{x}|^2$, yielding

$$\widehat{\mathbf{x}}' = \left(\mathbf{\Psi_P}^T\mathbf{\Psi_P}\right)^{-1}\mathbf{\Psi_P}^T\mathbf{r}'. \tag{12}$$

In order that $\left(\mathbf{\Psi_P}^T\mathbf{\Psi_P}\right)^{-1}$ exists, we need $N \le K_P$. Finally, the phase estimate is given by

$$\begin{aligned}\widehat{\boldsymbol{\theta}} &= \theta_{\text{avg}}\mathbf{1_K} + \mathbf{\Psi_K}\widehat{\mathbf{x}}' \\ &= \theta_{\text{avg}}\mathbf{1_K} + \mathbf{M}\mathbf{r}',\end{aligned} \tag{13}$$

where $\mathbf{M} = \mathbf{\Psi_K}\left(\mathbf{\Psi_P}^T\mathbf{\Psi_P}\right)^{-1}\mathbf{\Psi_P}^T$ and $(\widehat{\boldsymbol{\theta}})_k = \widehat{\theta}(k)$, $(\mathbf{1_K})_k = 1$, $(\mathbf{\Psi_K})_{k,n} = \psi_n(k)$, $k = 0,\ldots, K-1$; $n = 0,\ldots,N-1$. Note from (13) that the estimation algorithm does not need specific knowledge about the phase noise process. As $r'(k_i)$ from (11) can be viewed as a noisy version of $\theta(k_i) - \theta_{\text{avg}}$, the phase estimate $\widehat{\theta}$ from (13), or, equivalently, the phase estimate $\widehat{\boldsymbol{\theta}}(k)$ from (6), can be interpreted as an interpolated version of the subsampled noisy phase trajectory. The estimation of the phase trajectory involves the inversion of the $N\times N$ matrix $\mathbf{\Psi_P}^T\mathbf{\Psi_P}$, which depends on the pilot symbol positions $\{k_i, i = 0,\ldots,K_P-1\}$. Now, we point out that the pilot symbol positions can be selected such that $\mathbf{\Psi_P}^T\mathbf{\Psi_P}$ is diagonal, or, equivalently, that the N columns of the $K_P \times N$ matrix $\mathbf{\Psi_P}$ are orthogonal. Such selection of $\{k_i\}$ avoids the need for matrix inversion in (12). Denoting by $\phi_n(i)$ the orthonormal DCT basis functions of length K_P, it is easily verified that selecting $\{k_i\}$ such that

$$k_i = \frac{iK}{K_P} + \frac{K-K_P}{2K_P}, \quad i = 0,\ldots,K_P-1 \tag{14}$$

gives rise to

$$\psi_n(k_i) = \sqrt{\frac{K_P}{K}}\phi_n(i) \quad \text{for } n = 0,\ldots,K_P-1, \tag{15}$$

so that

$$\mathbf{\Psi_P}^T\mathbf{\Psi_P} = \frac{K_P}{K}\mathbf{I}_N \tag{16}$$

with $\mathbf{I}_N$ denoting the $N \times N$ identity matrix. Equations (12) and (13) then reduce to

$$\widehat{\mathbf{x}}' = \frac{K}{K_P}\mathbf{\Psi_P}^T\mathbf{r}', \tag{17}$$

$$\widehat{\theta} = \theta_{\text{avg}}\mathbf{1_K} + \frac{K}{K_P}\mathbf{\Psi_K}\mathbf{\Psi_P}^T\mathbf{r}'. \tag{18}$$

In order that all k_i from (14) be integer, K must be an odd multiple of K_P, that is, $K = (2d+1)K_P$, yielding $k_i = (2d+1)i+d$. The resulting pilot symbol configuration is suited for estimating any number of DCT coefficients not exceeding K_P. When K is not an odd multiple of K_P, rounding the right-hand side of (14) to the nearest integer gives rise to pilot symbol positions that still yield an essentially diagonal matrix $\mathbf{\Psi_P}^T\mathbf{\Psi_P}$ in which case the simplified equations (17) and (18) can still be used.

3. Performance Analysis

As the observation vector $\mathbf{r}_P$ is a nonlinear function of the carrier phase, an exact analytical performance analysis is not feasible. Instead, we will resort to a linearization of the argument function in (11) in order to obtain tractable results.

Linearization of the argument function yields

$$\begin{aligned}r'(i) &= \arg\left(r(k_i)a^*(k_i)e^{-j\theta_{\text{avg}}}\right) \\ &= \arg\left(e^{j(\theta(k_i)-\theta_{\text{avg}})}\left(E_s + a^*(k_i)w(k_i)e^{-j\theta(k_i)}\right)\right) \\ &\approx \theta(k_i) - \theta_{\text{avg}} + n_P(i)\end{aligned} \tag{19}$$

for $i = 0,\ldots,K_P-1$, where $\{n_P(i)\}$ is a sequence of i.i.d. zero-mean Gaussian random variables with variance $N_0/2E_s$. Note that (19) incorporates the true phase $\theta(k_i)$ instead of the approximate model (4), so that our performance analysis will take the modeling error into account. In order that the linearization in (19) be valid, we need $|\theta(k_i) - \theta_{\text{avg}}| < \pi$ (because $|\arg(z)| < \pi$) and $|w(k_i)|^2 \ll E_s$; hence, the phase noise fluctuations should not cause phase wrapping and E_s/N_0 should be sufficiently large. Substituting (19) into (13) yields

$$\widehat{\boldsymbol{\theta}} = \mathbf{M}(\boldsymbol{\theta}_P + \mathbf{n}_P) = \mathbf{M}\mathbf{S}\boldsymbol{\theta} + \mathbf{M}\mathbf{n}_P, \tag{20}$$

where $(\mathbf{n}_P)_i = n_P(i)$, $(\boldsymbol{\theta}_P)_i = \theta(k_i)$, and the $K_P \times K$ matrix $\mathbf{S}$ is such that its ith row has a 1 at the k_ith column and zeroes elsewhere $(i = 0, \ldots, K_P - 1)$. The estimation error resulting from (20) is given by

$$\widehat{\boldsymbol{\theta}} - \boldsymbol{\theta} = (\mathbf{MS} - \mathbf{I_K})\boldsymbol{\theta} + \mathbf{Mn}_P, \tag{21}$$

where $\mathbf{I_K}$ denotes the $K \times K$ identity matrix. If the model (4) was exact, we would have $\boldsymbol{\theta} = \boldsymbol{\Psi}_\mathbf{K}\mathbf{x}$ and $\boldsymbol{\theta}_P = \boldsymbol{\Psi}_\mathbf{P}\mathbf{x}$, yielding

$$\widehat{\boldsymbol{\theta}} = \boldsymbol{\theta} + \mathbf{Mn}_P, \tag{22}$$

in which case the estimation error would be caused only by the additive noise.

As a performance measure of the estimation algorithm, we consider the mean-square error (MSE), defined as

$$\text{MSE} = \frac{1}{K} E\left[\operatorname{trace}\left((\widehat{\boldsymbol{\theta}} - \boldsymbol{\theta})(\widehat{\boldsymbol{\theta}} - \boldsymbol{\theta})^T\right)\right]. \tag{23}$$

Substituting (21) into (23) yields

$$\text{MSE} = \frac{1}{K}\frac{N_0}{2E_s}\operatorname{trace}\left(\left({\boldsymbol{\Psi}_\mathbf{P}}^T\boldsymbol{\Psi}_\mathbf{P}\right)^{-1}\right) + \text{MSE}_\infty, \tag{24}$$

where

$$\text{MSE}_\infty = \frac{1}{K}\operatorname{trace}\left((\mathbf{MS} - \mathbf{I_K})\mathbf{R}_\theta(\mathbf{MS} - \mathbf{I_K})^T\right). \tag{25}$$

The first term in (24) denotes the contribution from the additive noise, whereas the second term in (24) constitutes an MSE floor, caused by the phase noise modeling error. The phase noise statistics affect the MSE floor through the autocorrelation matrix $\mathbf{R}_\theta$. The MSE floor decreases with increasing N (because the modeling error is reduced when more DCT coefficients are taken into account), whereas the additive noise contribution to the MSE increases with N (because N parameters need to be estimated). Hence, there is an optimum value of N that minimizes the MSE.

From the nonlinear observation model (7), which assumes that (4) holds with equality, we compute the Cramer-Rao lower bound on the MSE (23) resulting from any unbiased estimate $\hat{\mathbf{x}}$ of the DCT coefficients of $\theta(k)$:

$$\text{MSE} \geq \frac{1}{K}\operatorname{trace}(\mathbf{J}^{-1}). \tag{26}$$

In (26), $\mathbf{J}$ denotes the Fisher information matrix related to the estimation of $\mathbf{x}$ from (7), which is found to be

$$(\mathbf{J})_{n,n'} = \frac{2E_s}{N_0}\left(\left({\boldsymbol{\Psi}_\mathbf{P}}^T\boldsymbol{\Psi}_\mathbf{P}\right)^{-1}\right)_{n,n'}. \tag{27}$$

Combining (26) with (27) yields the following performance bound:

$$\text{MSE} \geq \frac{1}{K}\frac{N_0}{2E_s}\operatorname{trace}\left(\left({\boldsymbol{\Psi}_\mathbf{P}}^T\boldsymbol{\Psi}_\mathbf{P}\right)^{-1}\right). \tag{28}$$

Comparison of (24) and (28) indicates that our ad hoc algorithm (13) yields the minimum possible (over all unbiased estimates) noise contribution to the MSE (assuming that the linearization of the observation model is valid).

When the pilot symbol positions $\{k_i\}$ are selected according to (14), the Cramer-Rao bound (28) reduces to

$$\text{MSE} \geq \frac{N_0}{2E_s}\frac{N}{K_P}, \tag{29}$$

which indicates that the sensitivity to additive noise increases with the number (N) of estimated DCT coefficients.

4. Frequency-Domain Analysis

After linearization, (20) relates the phase estimate $\widehat{\boldsymbol{\theta}}$ to the actual phase $\boldsymbol{\theta}$ and the additive noise $\mathbf{n}_P$. In the absence of additive noise, the estimator can be viewed as a linear system that transforms $\boldsymbol{\theta}$ into $\widehat{\boldsymbol{\theta}}$ by means of the transfer matrix $\mathbf{MS}$. In order to analyze this system in the frequency domain, we consider an input $\boldsymbol{\theta}_n$ with $(\boldsymbol{\theta}_n)_k = \exp(j2\pi kn/K)$, that is, $\boldsymbol{\theta}_n$ contains only the frequency n/K. We investigate the mean-square error MSE_n between the input $\boldsymbol{\theta}_n$ and the output $\widehat{\boldsymbol{\theta}} = \mathbf{MS}\theta_n$; MSE_n is given by (25), with $\mathbf{R}_\theta$ replaced by $\boldsymbol{\theta}_n\boldsymbol{\theta}_n^H$, where the superscript H indicates conjugate transpose.

As $\boldsymbol{\theta}_n$ is periodic in n with period K, the same periodicity holds for MSE_n. Assuming the pilot symbol positions are according to (14) with $K = 105$ and $Kp = 15$, Figure 1 shows MSE_n as a function of n/K, with n/K in the interval $[-1/2, 1/2]$ and $N = 7$. The behavior of MSE_n is explained by noting that subsampling $\boldsymbol{\theta}_n$ at the instants k_i (with spacing K_P) gives rise to aliasing. Frequencies n/K and $(n + K_P)/K$ yield the same subsampled phase trajectory. In the following discussion, the intervals I_{K_P} and I_N are defined as $[-(K_P - 1)/(2K), (K_P - 1)/(2K)]$ and $[-(N-1)/(2K), (N-1)/(2K)]$, respectively; note that $I_N \subset I_{K_P}$.

(i) As the first N basis functions of the DCT transform cover the frequency interval I_N, we get $\widehat{\boldsymbol{\theta}}_n \approx \boldsymbol{\theta}_n$ and $\text{MSE}_n \approx 0$ when n/K is in I_N.

(ii) When n/K is in the interval I_{K_P}, but outside I_N, we get $\widehat{\boldsymbol{\theta}}_n \approx 0$ and $\text{MSE}_n \approx 1$.

(iii) Suppose $n = mK_P + n'$, with $m \neq 0$, $|m| < K/(2K_P)$ and n' in I_{K_P}, because of aliasing, $\boldsymbol{\theta}_n$ is interpreted as $\boldsymbol{\theta}_{n'}\exp(j\phi_m)$ with $\phi_m = 2\pi m(K - K_P)/(2K)$. When n' is in the interval I_N, we get $\widehat{\boldsymbol{\theta}}_n \approx \boldsymbol{\theta}_{n'}\exp(j\phi_m)$. The resulting estimation error is the sum of two complex exponentials with frequencies n/K and n'/K, yielding $\text{MSE}_n \approx 2$. When n' is not in I_N, we get $\widehat{\boldsymbol{\theta}}_n \approx 0$ and $\text{MSE}_n \approx 1$.

It follows from Figure 1 that the estimator can be viewed as a low-pass system with bandwidth $B = (N-1)/(2K)$. Basically, the frequency components n/K of $\boldsymbol{\theta}$ with $|n/K| < B$ are tracked by the estimator, whereas the components with $|n/K| > B$ contribute to the MSE.

5. Simulation Results

In this section, we assess the performance of the proposed technique in terms of the MSE of the phase estimate and the resulting BER degradation by means of computer simulations. In our simulations, we will consider two types of phase noise, that is, Wiener phase noise and first-order phase noise. The (discrete time) first-order phase noise process $\theta(k)$ can be viewed as the output of a one-pole filter driven by white Gaussian noise:

$$\theta(k+1) = (1-\alpha)\theta(k) + \Delta(k), \tag{30}$$

where $\{\Delta(k)\}$ is a sequence of i.i.d. zero-mean Gaussian random variables with variance σ_Δ^2. The corresponding phase noise power spectrum and phase noise variance are given by

$$\begin{aligned} S_\theta^{\text{1st-order}}\left(e^{j2\pi fT}\right) &= \frac{\sigma_\Delta^2}{\left|\exp(j2\pi fT) - 1 + \alpha\right|^2} \\ &\approx \frac{\sigma_\Delta^2}{|j2\pi fT + \alpha|^2}, \end{aligned} \tag{31}$$

$$\sigma_\theta^2 = \frac{\sigma_\Delta^2}{\alpha(2-\alpha)} \approx \frac{\sigma_\Delta^2}{2\alpha}. \tag{32}$$

The approximations in (31) and (32) hold for $fT \ll 1/2$ and $\alpha \ll 1$. It follows from (31) that $\alpha/2\pi T$ is the 3 dB frequency of the power spectrum. The first-order phase noise models the phase instabilities of an oscillator signal that results from a phase-locked loop (PLL) circuit. The (discrete-time) Wiener phase noise $\theta(k)$ is described by the following system equation:

$$\theta(k+1) = \theta(k) + \Delta(k), \quad k = 0,\ldots,K-2, \tag{33}$$

where the initial phase noise value $\theta(0)$ is uniformly distributed in $[-\pi,\pi]$ and $\Delta(k)$ has the same meaning as in (30). Hence, $\theta(k)$ can be viewed as the output of an integrator with a white noise input. From (33), it follows that the variance of the Wiener phase noise increases linearly with the time index k, which indicates that the process is nonstationary.

Comparing (33) and (30), it follows that the Wiener phase noise can be interpreted as a limiting case of first-order phase noise, in the limit for $\alpha \to 0$. Hence, one can *formally* define the Wiener phase noise spectrum as the limit of the first-order spectrum (31); for $\alpha \to 0$,

$$S_\theta^{\text{Wiener}}\left(e^{j2\pi fT}\right) = \frac{\sigma_\Delta^2}{\left|\exp(j2\pi fT) - 1\right|^2} \approx \frac{\sigma_\Delta^2}{4\pi^2 f^2 T^2}, \tag{34}$$

where the approximation in (34) holds for $|fT| \ll 1/2$. Note that the Wiener phase noise spectrum becomes unbounded at $f = 0$, which is a consequence of the variance increasing linearly with time. In contrast, the complex envelope $\exp(j\theta)$ of the oscillator signal can be shown to be a stationary process (with [1, the Lorentzian power spectrum]). The Wiener phase noise model is often used to describe the phase noise process of a free-running oscillator, although also more elaborate models exist, involving a phase noise spectrum that consists of a sum of terms of the form $A_m f^{-m}$, $m = 0,\ldots,4$ [10, 17–19]. In order to reduce the strong low-frequency components of the phase noise resulting from a free-running oscillator, the oscillator is often incorporated in a PLL circuit;

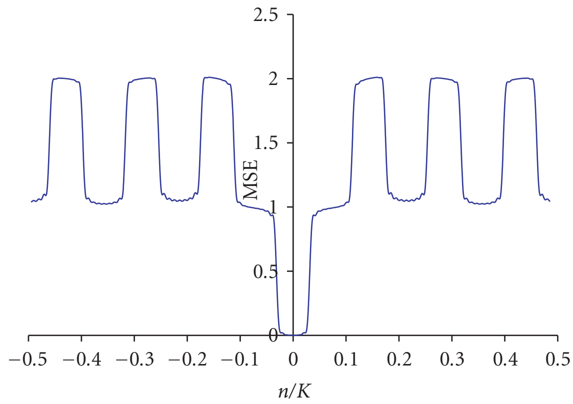

Figure 1: MSE as a function of n/K for $K = 105$, $K_P = 15$, and $N = 7$.

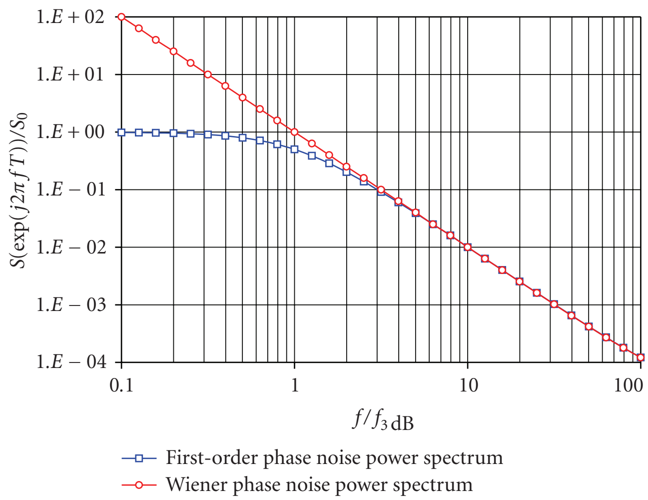

Figure 2: Power spectrum for Wiener phase noise and first-order phase noise.

a first-order PLL gives rise to the first-order phase noise process (30) [17].

Figure 2 shows the first-order phase noise power spectrum, normalized by its value S_0 at $f = 0$, as a function of the normalized frequency $f/f_{3\,\text{dB}}$, with $f_{3\,\text{dB}} = \alpha/(2\pi T)$; also displayed is the Wiener phase noise power spectrum (normalized by the same S_0). As for both types of phase noise, the same value of σ_Δ^2 has been used, both spectra have the same high-frequency content.

In the following simulations, Wiener phase noise is assumed, unless noted otherwise. First, we assume transmission of a block of length $K = 105$ symbols, consisting of $K_D = 90$ uncoded QPSK data symbols and $K_P = 15$ constant-energy pilot symbols that are inserted into the sequence according to (14).

(i) Figure 3 shows the MSE of the phase estimate in the absence of phase noise as a function of E_s/N_0 when $N = 1, 4$ and 10 DCT coefficients are estimated; in addition, these simulation results are compared to the corresponding CRB (29). We observe that the CRB is achieved for sufficiently

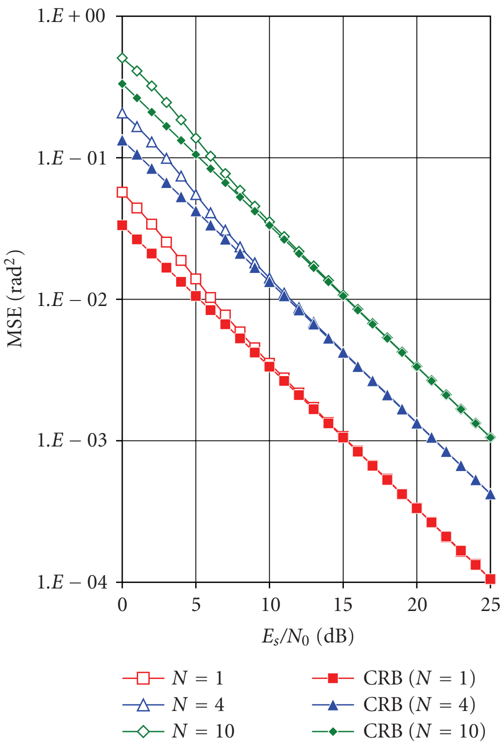

FIGURE 3: MSE in the absence of phase noise compared to the corresponding CRB. $K = 105$, $K_P = 15$.

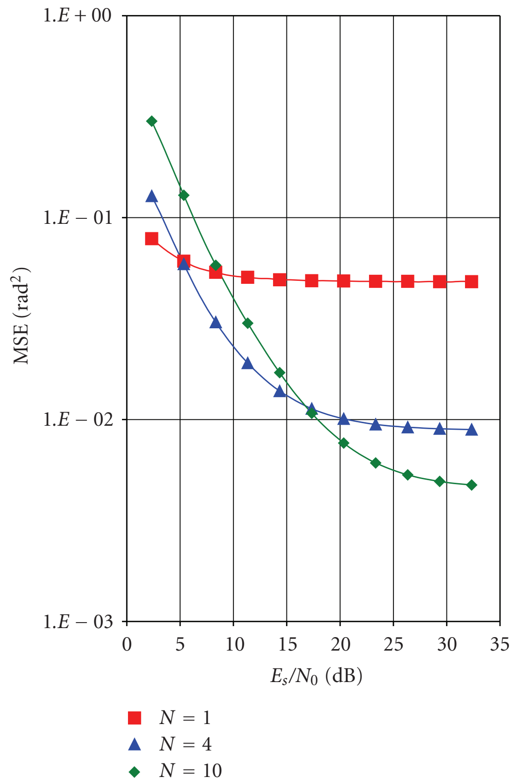

FIGURE 4: MSE when Wiener phase noise with $\sigma_\Delta = 3°$ is present $K = 105$, $K_P = 15$.

high values of E_s/N_0. For small E_s/N_0, the MSE exceeds the CRB, which is in agreement with the fact that the linearized observation model from (19) is no longer accurate in the low-SNR region. Furthermore, it is confirmed that the contribution from the additive noise to the MSE is proportional to the number of estimated coefficients N.

(ii) Figure 4 shows the MSE as a function of E_s/N_0 for $N = 1, 4$ and 10, but this time in the presence of Wiener phase noise with $\sigma_\Delta^2 = 0.0027\,\text{rad}^2$ (which corresponds to "strong" phase noise, with $\sigma_\Delta = 3°$). We observe an MSE floor in the high-E_s/N_0 region, which can be reduced by increasing the number N of estimated coefficients. Figure 4 also confirms that for low E_s/N_0, the MSE increases when N increases. This high-E_s/N_0 and low-E_s/N_0behaviors indicate that for given K, K_P, and E_s/N_0, the MSE can be minimized by proper selection of N.

(iii) Figure 5 shows the bit error rate (BER) as a function of E_b/N_0 (E_b is the energy per transmitted bit, $E_s = 2(1-\eta)E_b$ for QPSK) for $N = 1, 4$, and 10. The reference BER curve corresponds to a system with perfect synchronization and no pilot symbols ($\eta = 0$). We observe that for low E_b/N_0, it is sufficient to estimate only the time-average of the phase (i.e., $N = 1$). Estimating a higher number of DCT coefficients can lead to a worse BER performance for low E_b/N_0 because the MSE of the phase estimate due to additive noise increases with N. At high E_b/N_0, a BER floor occurs which decreases with increasing N, so in this region it becomes beneficial to estimate more than just one DCT coefficient. Hence, the optimal number of estimated coefficients N_{opt} will depend on the operating E_b/N_0.

(iv) Figure 6 compares the BER degradations at $\text{BER}_{\text{ref}} = 10^{-4}$ resulting from Wiener phase noise and first-order phase noise; the value of σ_Δ^2 is the same for both phase noise processes, such that the Wiener phase noise spectrum and first-order phase noise spectrum are the same for large f. (The BER degradation caused by some impairment is characterized by the increase (in dB) of E_b/N_0 (as compared to the case of no impairment) needed to maintain the BER at a specified reference level.) As the 3 dB frequency $\alpha/(2\pi T)$ of the first-order phase noise is less than BT, the frequency contents of the Wiener phase noise and the first-order phase noise outside the estimator bandwidth are essentially the same, and the corresponding BER curves are nearly coincident; this is in agreement with the analysis from Section 4, where we showed that the low-frequency components of the phase noise practically do not contribute to the phase error. It is also confirmed that there is an optimum value of N that minimizes the BER degradation; this optimum N increases with σ_Δ.

Next, we study the influence of the pilot symbol positions in the symbol sequence, assuming Wiener phase noise with $\sigma_\Delta = 3°$. The following scenarios are considered (see Figure 7), with $K_P = 15$.

(i) The pilot symbols are inserted according to (14) (SCEN1).

(ii) All pilot symbols are located in the middle of the sequence (SCEN2).

(iii) $\lceil K_P/2 \rceil$ pilot symbols are inserted at the beginning of the sequence, the remaining $\lfloor K_P/2 \rfloor$ pilot symbols are placed at the end (SCEN3).

(iv) The K_P pilot symbols are placed equidistantly at positions $\{0, K/K_P, ..., (K_P - 1)K/K_P\}$ (SCEN4).

(v) We divide the total number of 15 pilot symbols into 3 clusters of 5 consecutive pilot symbols each. The 3 clusters are centered at the positions (14) that correspond to $K_P = 3$ (SCEN5).

(vi) We divide the total number of 15 pilot symbols into 5 clusters of 3 consecutive pilot symbols each. The 5 clusters are centered at the positions (14) that correspond to $K_P = 5$ (SCEN6).

Figure 8 shows the BER for each scenario with $N = 4$. We observe that SCEN2 and SCEN3 lead to essentially the same BER performance, that turns out to be very poor. The BER resulting from SCEN5 is slightly better, but still poor. Much better BER performance is obtained for SCEN1, SCEN4, and SCEN6, with SCEN1 yielding the best performance. The poor performance resulting from SCEN2, SCEN3, and SCEN5 comes from the poor conditioning of the 15×4 matrix $\mathbf{\Psi_P}$, yielding very large values when computing the inverse of $\mathbf{\Psi_P}^T\mathbf{\Psi_P}$. As the DCT basis functions $\psi_0(k), \ldots, \psi_3(k)$ change only slowly with k, SCEN2 yields a matrix $\mathbf{\Psi_P}$ with nearly identical rows, so it behaves like a matrix of rank 1. Similarly, the matrices $\mathbf{\Psi_P}$ that correspond to SCEN3 and SCEN5 behave like matrices of ranks 2 and 3, respectively. Hence, when the pilot symbols are placed in a number of clusters that are less than the number (N) of DCT coefficients to be estimated, poor performance results. For SCEN1, SCEN4, and SCEN6, the number of pilot symbol clusters exceeds N; the corresponding matrices $\mathbf{\Psi_P}$ are full-rank (rank = 4), and good performance results. Note that SCEN1 and SCEN4 can cope with values of N up to K_P, whereas SCEN6 cannot handle values of N in excess of 5.

In the following, we investigate the influence of the number of pilot symbols on the MSE and the BER. The constant-energy pilot symbols are inserted into the data sequence according to (14). For (14) to hold, the block length K should be an odd multiple of the number of pilot symbols K_P. We assume a total block length $K = 105$ and simulate the BER and MSE for $K_P = 7, 15,$ and 35. Figure 9 shows the BER degradation at BER$= 10^{-4}$ with respect to the reference system, for a fixed ratio $\eta = K_P/K = 20\%$ and various values of the block length K. The BER degradation $-10\log(1 - \eta)$ due to the insertion of pilot symbols (which amounts to 0.97 dB for $\eta = 0.2$) is included. The following observation can be made.

(i) For given block size K, there is an optimum number N_{opt} of DCT coefficients to be estimated that minimizes the BER degradation. This is consistent with the observation that the MSE of the phase estimate can be minimized by a suitable choice of N.

(ii) For very small K, $N_{\text{opt}} = 1$. The optimum value N_{opt} increases with increasing K because more DCT coefficients

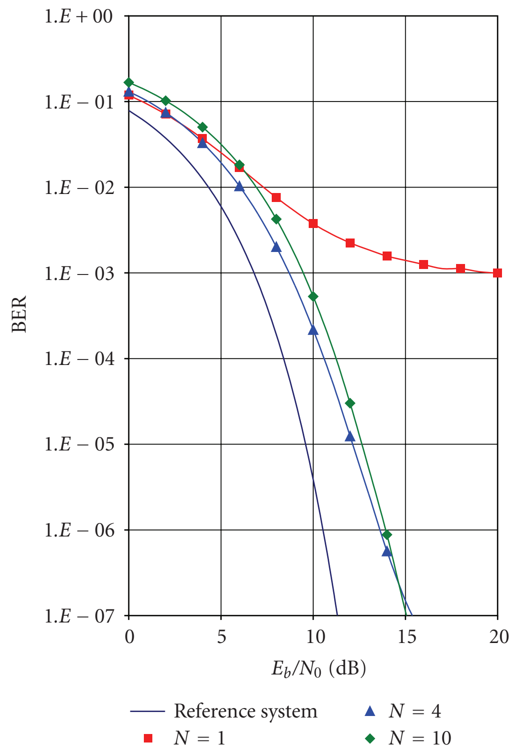

Figure 5: BER when Wiener phase noise with $\sigma_\Delta = 3^\circ$ is present. $K = 105$, $K_P = 15$.

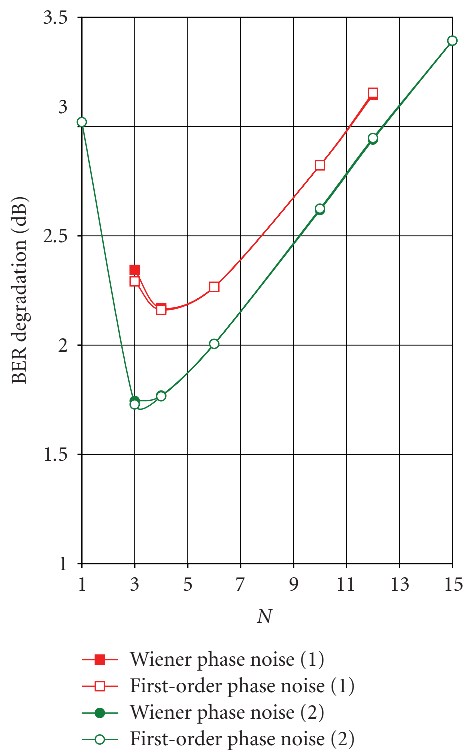

Figure 6: BER degradation as a function of the number of estimated coefficients N for Wiener phase noise and first-order phase noise with $\alpha = 0.015$. (1) $\sigma_\Delta^2 = 0.0027\,\text{rad}^2$; (2) $\sigma_\Delta^2 = 0.0015\,\text{rad}^2$. $K = 105$, $K_P = 15$.

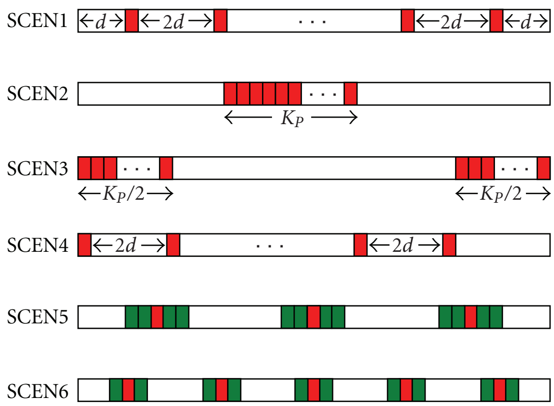

Figure 7: Pilot symbol insertion schemes.

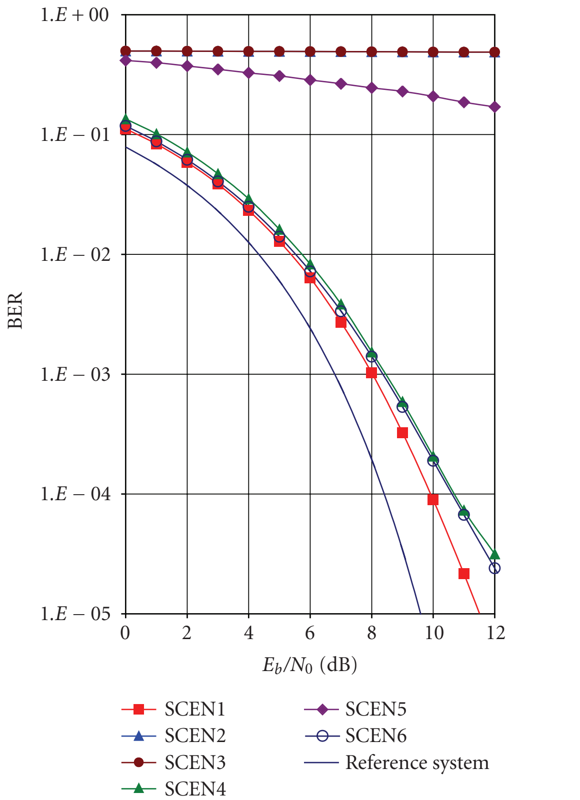

Figure 8: BER for different pilot symbol placement scenarios. $K = 105$, $K_P = 15$, $N = 4$.

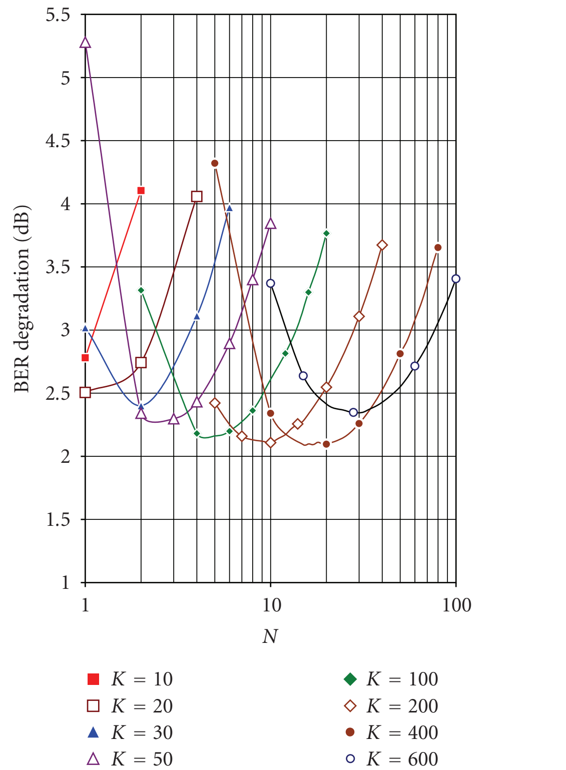

Figure 9: BER degradation for BER $= 10^{-4}$ as function of N for various K and fixed pilot symbol ratio $\eta = K_P/K = 20\%$ and $\sigma_\Delta = 3^\circ$.

are needed to model the phase fluctuations when K gets larger. Keeping $N = 1$ yields very large degradations when K increases.

(iii) The BER degradation that corresponds to $N = N_{\text{opt}}$ exhibits a (broad) minimum as a function of K. As long as the fluctuation of $\theta(k)$ about its time-average is small, so that linearization of the argument function in (11) applies, the degradation decreases with increasing K because the number K_P of noisy observations of the phase noise increases when the ratio K_P/K is fixed. However, for too large K, the fluctuation of the Wiener phase noise is so large that linearization is no longer valid (for Wiener phase noise, we need $K\sigma_\Delta^2 \ll 1$ for the linearization to be accurate) and the resulting degradation increases with increasing K.

For the considered scenario, the minimum degradation occurs at $(K_{\text{opt}}, N_{\text{opt}}) \approx (400, 20)$ and amounts to about 2.1 dB. When the actual block size K exceeds K_{opt}, the degradation can be limited by dividing the block in subblocks of at most K_{opt} symbols, and estimating the phase trajectory for each subblock separately.

Figure 10 shows the BER degradation when (1) $\eta = 20\%$ and $\sigma_\Delta = 3^\circ$ and (2) $\eta = 10\%$ and $\sigma_\Delta = 2^\circ$, for the following phase noise estimation algorithms.

(i) The proposed DCT-based algorithm with pilot symbol placement according to SCEN1 (14) and selection of the optimum N.

(ii) Estimation of only the time-average of the phase noise, with the pilot symbols arranged according to SCEN3.

(iii) The method from Luise et al. [11], with the pilot symbols arranged according to SCEN3. The phase noise over the total symbol block is approximated as a linear interpolation between the average phase values over the first and the second pilot symbol clusters .

We observe that estimating only the time-average or the linear trend of the phase noise yields poor BER performance, except for small K. For $K = 10$, the DCT-based algorithm

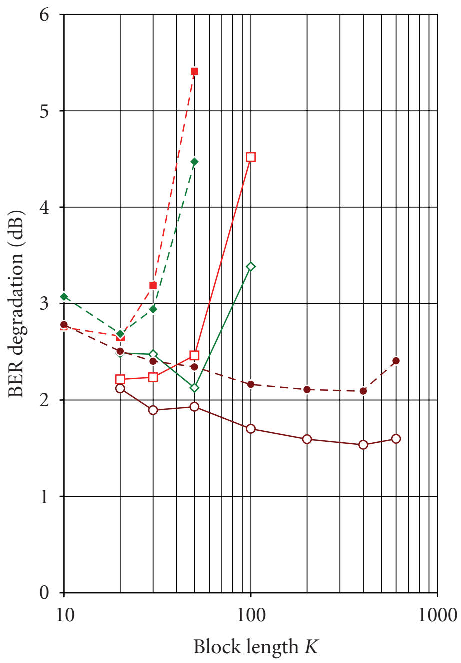

Figure 10: Comparison of BER degradation for BER $= 10^{-4}$ as function of K. (1) $\eta = 20\%$ and $\sigma_\Delta = 3^\circ$; (2) $\eta = 10\%$ and $\sigma_\Delta = 2^\circ$.

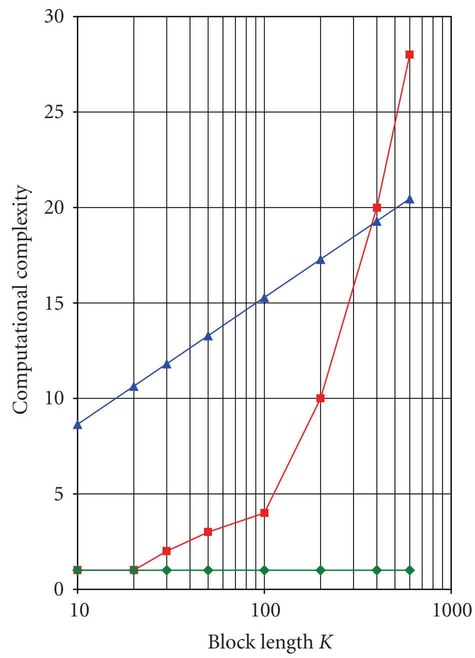

Figure 11: Complexity comparison for the proposed algorithm (approaches 1 and 3) and for Luise et al. algorithm.

also estimates the time-average only (because $N = 1$ is optimum for $K = 10$); we observe that SCEN3 (with pilot symbols at positions 0 and 9) performs slightly better than the DCT-based algorithm (with pilot symbols at positions 2 and 7) for $K = 10$. However, when the block length is increased, the DCT algorithm that estimates multiple DCT coefficients outperforms both SCEN3 and Luise et al. and leads to a BER degradation that decreases with increasing K until an optimal value for K is reached.

6. Complexity Analysis

In order to assess the complexity of the proposed algorithm, we determine the number of complex multiplications required per symbol interval. The calculation of the second term in (18) requires the highest number of computations. This term can be evaluated in the following ways.

(1) In a first approach, $(K/K_P)\mathbf{\Psi_K}\mathbf{\Psi_P}^T\mathbf{r}'$ is calculated via two matrix multiplications: first $\mathbf{\Psi_P}^T$ (dimension $N \times K_P$) and $\mathbf{r}'$ (dimension $K_P \times 1$) are multiplied and then $(K/K_P)\mathbf{\Psi_K}$ (dimension $K \times N$)and $\mathbf{\Psi_P}^T\mathbf{r}'$ (dimension $N \times 1$) are multiplied. The resulting complexity is of the order $O(NK_P + KN) \approx O(KN)$, with the approximation holding for $K \gg K_P$. Hence, the complexity per symbol interval amounts to $O(N)$.

(2) In a second approach, $(K/K_P)\mathbf{\Psi_K}\mathbf{\Psi_P}^T\mathbf{r}'$ is calculated via a single-matrix multiplication: $(K/K_P)\mathbf{\Psi_K}\mathbf{\Psi_P}^T$ (dimension $K \times K_P$) and $\mathbf{r}'$ (dimension $K_P \times 1$) are multiplied. Taking into account that $(K/K_P)\mathbf{\Psi_K}\mathbf{\Psi_P}^T$ can be computed offline, the resulting complexity per symbol is $O(K_P)$. As $N \leq K_P$, the first approach is to be preferred over the second approach.

(3) The third approach exploits the fact that $\mathbf{\Psi_K}$ and $\mathbf{\Psi_P}$ are submatrices of $K \times K$ and $K_P \times K_P$ DCT transform matrices, respectively. Hence, the two matrix multiplications from the first approach can be replaced by an inverse DCT transform (size K_P) followed by a DCT transform (size K). As $K \gg K_P$, the complexity of the size-K DCT dominates. The DCT of a vector $\{s(0), s(1), \dots, s(K-1)\}$ of length K can be obtained by calculating the discrete Fourier transform (DFT) of its even expansion $\{s(K-1), \dots, s(1), s(0), s(0), s(1), \dots, s(K-1)\}$ (note that the even expansion has length $2K$). As the FFT algorithm used for calculating the DFT of length M has a computational complexity $O(M\log_2(M))$, the complexity of the size- K DCT is $O(2K\log_2(2K))$, yielding a complexity per symbol interval of $O(\log_2(4K^2))$.

The complexity per symbol interval of the phase noise estimation method used by Benvenuti et al. [11] is about $O(1)$. Figure 11 shows the order of complexity as a function of the block length K, for the proposed algorithm (approaches 1 and 3) and for Luise et al. algorithm; the result related to the first approach in the proposed algorithm corresponds to taking for each K the value of N that is optimum for $\sigma_\Delta = 3^\circ$. Luise et al. algorithm has a smaller complexity than the proposed algorithm, but the latter algorithm outperforms the former, especially when the phase noise is strong. For the proposed algorithm, we notice that matrix multiplication according to the first approach leads to the lowest computational complexity for $K < 400$. As K becomes larger than 400, calculation via FFT (third approach) is less complex. At the point $(K_{\text{opt}}, N_{\text{opt}}) = (400, 20)$ yielding minimum BER degradation (see Figure 9), the first and third approaches give rise to the same complexity.

7. Conclusions and Remarks

In this contribution, we have considered an ad hoc feed-forward data-aided phase noise estimation algorithm that is based on the estimation of only a few (N) coefficients of the DCT basis expansion of the time-varying phase. The algorithm does not require detailed knowledge about the phase noise statistics. Linearization of the observation model has indicated that the mean-square error of the resulting estimate consists of an additive noise contribution (that increases with N) and an MSE floor caused by the phase noise modeling error (that decreases with N). The noise contribution coincides with the Cramer-Rao lower bound.

These analytical findings have been confirmed by means of computer simulations. The influence of the position and number K_P of pilot symbols inserted into the symbol sequence has been investigated. Computer simulations were carried out for several pilot symbol configurations. Arranging the pilot symbols according to (14), such that the subsampled DCT basis functions remain orthogonal, reduces the BER degradation as compared to the case of a preamble/postamble or midamble pilot symbol arrangement with estimation of only the time-average; in addition, the configuration (14) allows to estimate up to K_P DCT coefficients with a reduced computational complexity. The BER degradation can be minimized by a suitable choice of block length K, the number K_P of pilot symbols, and the number N of DCT coefficients to be estimated.

The considered DCT-based phase estimation algorithm makes use of the energy associated with the pilot symbols only. Further research will involve the incorporation of the DCT-based algorithm in an iterative phase noise estimation algorithm that exploits soft decisions about the data symbols, so that the resulting algorithm benefits from the energy associated with the data symbols as well. The performance and complexity of such an iterative algorithm will be investigated and compared to other iterative algorithms (such as those from [12–16]).

Acknowledgments

The authors wish to acknowledge the activity of the Network of Excellence in Wireless COMmunications (NEWCOM++) of the European Commission (Contract no. 216715) that motivated this work. This work is also supported by the FWO Project G.0047.06 Advanced space-time processing techniques for communication through multiantenna systems in realistic mobile channels.

References

[1] A. Demir, A. Mehrotra, and J. Roychowdhury, "Phase noise in oscillators: a unifying theory and numerical methods for characterization," *IEEE Transactions on Circuits and Systems I*, vol. 47, no. 5, pp. 655–674, 2000.

[2] T. E. Parker, "Characteristics and sources of phase noise in stable oscillators," in *Proceedings of the 41st Annual Frequency Control Symposium*, pp. 99–110, Philadelphia, Pa, USA, May 1987.

[3] G. B. Giannakis and C. Tepedelenlioglu, "Basis expansion models and diversity techniques for blind identification and equalization of time-varying channels," *Proceedings of the IEEE*, vol. 86, no. 10, pp. 1969–1986, 1998.

[4] J. K. Tugnait and W. Luo, "Blind space-time multiuser channel estimation in time-varying DS-CDMA systems," *IEEE Transactions on Vehicular Technology*, vol. 55, no. 1, pp. 207–218, 2006.

[5] O. Rousseaux, G. Leus, and M. Moonen, "Estimation and equalization of doubly selective channels using known symbol padding," *IEEE Transactions on Signal Processing*, vol. 54, no. 3, pp. 979–990, 2006.

[6] J.-C. Nallatamby, M. Prigent, E. Vaury, A. Laloue, M. Camiade, and J. Obregon, "Low phase noise operation of microwave oscillator circuits," *IEEE Transactions on Ultrasonics, Ferroelectrics and Frequency Control*, vol. 47, no. 2, pp. 411–420, 2000.

[7] J. Mukherjee, "Optimizing MOSFET channel width for low phase noise in LC oscillators," in *Proceedings of the 50th Midwest Symposium on Circuits and Systems (MWSCAS '07)*, pp. 610–613, Montreal, Canada, August 2007.

[8] D. Y. Jung and C. S. Park, "Power efficient Ka-band low phase noise VCO in 0.13 μm CMOS," *Electronics Letters*, vol. 44, no. 10, pp. 628–630, 2008.

[9] H. Meyr, M. Moeneclaey, and S. Fechtel, *Digital Communication Receivers: Synchronization, Channel Estimation, and Signal Processing*, Wiley Series in Telecommunications and Signal Processing, John Wiley & Sons, New York, NY, USA, 1998.

[10] U. Mengali and A. N. D'Andrea, *Synchronization Techniques for Digital Receivers*, Plenum Press, New York, NY, USA, 1997.

[11] L. Benvenuti, L. Giugno, V. Lottici, and M. Luise, "Code-aware carrier phase noise compensation on turbo-coded spectrally-efficient high-order modulations," in *Proceedings of the 8th International Workshop on Signal Processing for Space Communications (SPSC '03)*, pp. 177–184, Catania, Italy, September 2003.

[12] G. Colavolpe, A. Barbieri, and G. Caire, "Algorithms for iterative decoding in the presence of strong phase noise," *IEEE Journal on Selected Areas in Communications*, vol. 23, no. 9, pp. 1748–1757, 2005.

[13] J. Dauwels and H.-A. Loeliger, "Phase estimation by message passing," in *Proceedings of the IEEE International Conference on Communications (ICC '04)*, vol. 1, pp. 523–527, Paris, France, June 2004.

[14] E. Panayirci, H. Cirpan, and M. Moeneclaey, "A sequential Monte Carlo method for blind phase noise estimation and data detection," in *Proceedings of the 13th European Signal Processsing Conference (EUSIPCO '05)*, Antalya, Turkey, September 2005.

[15] E. Panayırcı, H. A. Çırpan, M. Moeneclaey, and N. Noels, "Blind-phase noise estimation in OFDM systems by sequential Monte Carlo method," *European Transactions on Telecommunications*, vol. 17, no. 6, pp. 685–693, 2006.

[16] S. Godtmann, N. Hadaschik, A. Pollok, G. Ascheid, and H. Meyr, "Iterative code-aided phase noise synchronization based on the LMMSE criterion," in *Proceedings of the 8th IEEE Signal Processing Advances in Wireless Communications (SPAWC '07)*, pp. 1–5, Helsinki, Finland, June 2007.

[17] D. Petrovic, W. Rave, and G. Fettweis, "Effects of phase noise on OFDM systems with and without PLL: characterization and compensation," *IEEE Transactions on Communications*, vol. 55, no. 8, pp. 1607–1616, 2007.

[18] ETSI, "Digital video broadcasting (dvb), second generation framing structure, channel coding and modulation systems for broadcasting, interactive services, news gathering and other broadband satellite applications".

[19] V. S. Abhayawardhana and I. J. Wassell, "Common phase error correction with feedback for OFDM in wireless communication," in *Proceedings of the IEEE Global Telecommunications Conference (GLOBECOM '02)*, vol. 1, pp. 651–655, Taipei, Taiwan, November 2002.

EURASIP Journal on Image and Video Processing

Special Issue on
Fast and Robust Methods for Multiple-View Vision

Call for Papers

Image and video processing has always been a hot research topic, and has many practical applications in areas such as television/movie production, augmented reality, medical visualization, and communication. Very often, multiple cameras are employed to capture images and videos of the scene at distinct viewpoints. In order to efficiently and effectively process such a large volume of images and videos, novel multiple-view image and video processing techniques should be developed.

The classical problem of multiple-view vision has been studied by a lot of researchers over the past few decades, and numerous solutions have been proposed to tackle the problem under various assumptions and constraints. Early methods developed in the 1980s and 1990s have laid down the foundations and theories for resolving the multiple-view vision problem. Nonetheless, many of these methods lack robustness and work well only under a well-controlled scene (e.g., homogeneous lighting, wide-baseline viewpoints, texture-rich surface).

Recently, a number of researchers revisit the multiple-view vision problem. Based on the well-developed theories on multiple-view geometry, they adopt robust implementations like statistical methods to produce solutions that can work well under general scene settings. Despite their robustness, these methods are often extremely computationally expensive and require days or even weeks to run and produce results. Therefore, efficient algorithms and implementations will be required to make those methods more practical. Techniques that are developed in real-time image/video processing can be redesigned and adapted for this interesting scenario.

This special issue targets at striking a balance between the efficiency and robustness of methods for multiple-view vision. This helps to bring multiple-view methods from laboratories to general home users. Topics of interest include, but are not limited to:

- Fast and robust feature detection and description
- Fast and robust feature matching and tracking
- Fast and robust camera calibration
- Efficient and precise image segmentation and registration
- Real-time 3D reconstruction/modeling
- Real-time texture and motion recovery
- Real-time robot navigation of dynamic scenes
- Multiview recognition algorithms
- Multiview vision algorithms for medical applications
- Stereo and multiview vision for 3D display and projection techniques
- Multiview image and geometry processing for 3D cinematography
- Compression and transmission of multiview video streams
- 3D video synchronization and optical modeling
- Video-based rendering in dynamic scenes
- Distributed and embedded algorithms for real-time geometry and video processing

Before submission, authors should carefully read over the journal's Author Guidelines, which are located at http://www.hindawi.com/journals/ivp/guidelines.html. Prospective authors should submit an electronic copy of their complete manuscripts through the journal Manuscript Tracking System at http://mts.hindawi.com/, according to the following timetable:

Manuscript Due	August 1, 2009
First Round of Reviews	November 1, 2009
Publication Date	February 1, 2010

Lead Guest Editor

Ling Shao, Philips Research Laboratories, 5656 AE Eindhoven, The Netherlands; l.shao@philips.com

Guest Editors

Amy Hui Zhang, United International College, Zhuhai, 519085 Guangdong, China; amyzhang@uic.edu.hk

Kenneth K. Y. Wong, Department of Computer Science, The University of Hong Kong, Hong Kong; kykwong@cs.hku.hk

Jiebo Luo, Kodak Research Laboratories, Rochester, NY 14650, USA; jiebo.luo@kodak.com

Hindawi Publishing Corporation
http://www.hindawi.com

International Journal of Digital Multimedia Broadcasting

Special Issue on Advances in 3DTV: Theory and Practice

Call for Papers

Extending visual content and communications with a third dimension, or otherwise capturing a dynamic scene in 3D and generating an optical duplicate of it at a remote site and in real-time, has been a dream over decades. The goal of the viewing experience is to create the illusion of a real environment in its absence, while all core and peripheral components related to this goal are collectively referred as three-dimensional television (3DTV). From a technological point of view, this goal targets advances over the whole 3DTV chain, including 3D image acquisition, 3D representation, compression, transmission, signal processing, interactive rendering, 3D display as well as customized 3DTV applications and spans a number of research fields from applied mathematics, computer science, and engineering. In a successful and consumer-accepted operation of 3DTV, the integration and interaction of all such functional components are required.

The objective of the proposed Special Issue is to present the works and efforts of researchers with diverse experience and activity in distinct, yet related and complementary areas, for achieving full-scale three-dimensional television.

Papers on the following and related list of topics are solicited, but are not limited to:

- 3D Capture and Processing
  - 3D time-varying scene capture technology, multicamera synchronization and recording, camera calibration and 3D view registration, holographic camera techniques, 3D motion analysis and tracking, surface modeling and segmentation, multiview image, and 3D data processing
- 3D Representation
  - Representation of 3D video information, volumetric and 3D mesh representation, texture and point representation, object-based representation and segmentation
- 3D Transmission
  - 3D data streaming, error-related issues and handling of 3D video, hologram compression, multiview video coding, 3D mesh compression, multiple description coding for 3D
- 3D Display
  - Stereoscopic and holographic display techniques, reduced parallax systems and integral imaging, optics and VLSI technology, projection and display technology for 3D videos, human factors
- 3D Applications
  - 3D imaging in cultural heritage and virtual archaeology, teleimmersion and remote collaboration, augmented reality and virtual environments, 3D television, cinema, games, and entertainment, biomedical applications, 3D content-based retrieval and recognition

Before submission, authors should carefully read over the journal's Author Guidelines, which are located at http://www.hindawi.com/journals/ijdmb/guidelines.html. Prospective authors should submit an electronic copy of their complete manuscript through the journal Manuscript Tracking System at http://mts.hindawi.com/, according to the following timetable:

Manuscript Due	May 1, 2009
First Round of Reviews	August 1, 2009
Publication Date	November 1, 2009

Lead Guest Editor

Xenophon Zabulis, Institute of Computer Science, Foundation for Research and Technology Hellas (FORTH), 700 13 Heraklion, Greece; zabulis@ics.forth.gr

Guest Editors

Irene Cheng, Department of Computing Science, University of Alberta, Edmonton, Alberta, Canada T6G 2E8; lin@cs.ualberta.ca

Nikolaos Grammalidis, Informatics and Telematics Institute, Centre of Research and Technology Hellas, 57001 Thessaloniki, Greece; ngramm@iti.gr

Georgios A. Triantafyllidis, Department of Applied Information and Multimedia, Technological Educational Institute of Crete, 710 04 Iraklio, Greece; gatrian@iti.gr

Pietro Zanuttigh, Department of Information Engineering, University of Padua, 35131 Padua, Italy; pietro.zanuttigh@dei.unipd.it

Special Issue on
Filter Banks for Next-Generation Multicarrier Wireless Communications

Call for Papers

Digital filter banks find various good applications in communications signal processing. In general, they can be used to obtain very sharp frequency selectivity to isolate different communications frequency channels from each other and from interfering spectral components. This can be done in a very flexible and dynamic manner. Thus, filter banks constitute a very powerful generic tool for software-defined radios and spectrally agile communication systems.

The theoretical capacity limits in communications can be approached by multicarrier techniques. With radio channels, multicarrier techniques can be combined with multiantenna transmitters and receivers to provide efficiency. Existing or planned transmission systems rely on the OFDM technique to reach these goals. However, OFDM has a number of drawbacks, such as the use of the cyclic prefix to cope with the channel impulse response which results in a loss of capacity and the requirement of block processing to maintain orthogonality among all the subcarriers. Furthermore, the leakage among frequency subbands has a serious impact on the performance of FFT-based spectrum sensing and OFDM-based cognitive radio in general.

So far, some attempts have been made to introduce filter bank multicarrier (FBMC) in the radio communications arena, in particular, the isotropic orthogonal transform algorithm (IOTA). However, the full exploitation and optimization of FBMC techniques in the context of radio evolution have not been considered sufficiently. Consequently, advances in communication aspects of FBMC are still required to make it useful for future radio systems.

This has motivated advanced research in the European ICT project PHYDYAS, which supports this special issue. Topics of interest include, but are not limited to:

- Filter bank-based multicarrier transmission and prototype filter design
- Filter bank-based signal processing for other communication waveforms
- Filter bank applications in software-defined radio
- Data-aided and blind techniques for synchronization and channel estimation
- Preamble and pilot-pattern design
- Equalization and demodulation
- FBMC MIMO techniques and beamforming
- Radio scene spectrum analysis and cognitive radio
- Interference management
- Interlayer optimization and FBMC-specific scheduling
- Filter bank for channel coding
- Filter bank in AD and DA conversions

Before submission authors should carefully read over the journal's Author Guidelines, which are located at http://www.hindawi.com/journals/asp/guidelines.html. Prospective authors should submit an electronic copy of their complete manuscript through the journal Manuscript Tracking System at http://mts.hindawi.com/, according to the following timetable:

Manuscript Due	June 1, 2009
First Round of Reviews	September 1, 2009
Publication Date	December 1, 2009

Lead Guest Editor

Markku Renfors, Department of Communications Engineering, Tampere University of Technology (TUT), 33720 Tampere, Finland; markku.renfors@tut.fi

Guest Editors

Pierre Siohan, Orange Labs 4, France Telécom, rue du Clos Courtel, BP 91226, 35512 Cesson Sévigné Cedex, France; pierre.siohan@orange-ftgroup.com

Behrouz Farhang-Boroujeny, Department of Electrical and Computer Engineering, University of Utah, 3280 MEB Salt Lake City, UT 84112, USA; farhang@ece.utah.edu

Faouzi Bader, Centre Tecnologic de Telecommunication de Catalunya (CTTC), Parc Mediterrani de la Tecnologia, Avenue Canal Olimpic, Casstelldefels, 08860 Barcelona, Spain; faouzi.bader@cttc.es